Proc. Natl. Acad. Sci. USA
Vol. 96, pp. 9391–9396, August 1999
Neurobiology

Molecular characterization of a slowly gating human hyperpolarization-activated channel predominantly expressed in thalamus, heart, and testis

REINHARD SEIFERT*†, ALEXANDER SCHOLTEN*, RENATE GAUSS*, ANTOANETA MINCHEVA‡, PETER LICHTER‡, AND U. BENJAMIN KAUPP*

*Institut für Biologische Informationsverarbeitung, Forschungszentrum Jülich, 52425 Jülich, Germany; and ‡Abteilung Organisation komplexer Genome, Deutsches Krebsforschungszentrum, 69120 Heidelberg, Germany

Communicated by Bert Sakmann, Max Planck Institute for Medical Research, Heidelberg, Germany, June 10, 1999 (received for review April 30, 1999)

ABSTRACT **Rhythmic activity of neurons and heart cells is endowed by pacemaker channels that are activated by hyperpolarization and directly regulated by cyclic nucleotides (termed HCN channels). These channels constitute a multigene family, and it is assumed that the properties of each member are adjusted to fit its particular function in the cell in which it resides. Here we report the molecular and functional characterization of a human subtype hHCN4. hHCN4 transcripts are expressed in heart, brain, and testis. Within the brain, the thalamus is the predominant area of hHCN4 expression. Heterologous expression of hHCN4 produces channels of unusually slow kinetics of activation and inactivation. The mean potential of half-maximal activation ($V_{1/2}$) was −75.2 mV. cAMP shifted $V_{1/2}$ by 11 mV to more positive values. The hHCN4 gene was mapped to chromosome band 15q24–q25. The characteristic expression pattern and the sluggish gating suggest that hHCN4 controls the rhythmic activity in both thalamocortical neurons and pacemaker cells of the heart.**

Ion channels activated by hyperpolarization and directly regulated by cyclic nucleotides (dubbed HCN channels; see ref. 1) play a fundamental role in shaping the autonomous rhythmic activity of single neurons and the periodicity of network oscillations (for reviews, see refs. 1–3). Among the best studied examples are the pacemaker currents in cells of the sinoatrial node (I_f) (4) and in relay neurons of the thalamus (I_h) (2). The thalamus is the major gateway for the flow of information toward the cerebral cortex, and it is the first station at which incoming signals can be blocked. During sleep, the rapid activity patterns characteristic of the aroused state are replaced by low-frequency, synchronized rhythms of neuronal activity. The physiological significance of the oscillatory modes is uncertain, but they may play a role in controlling the flow of information through the thalamus.

During early stage of quiescent sleep, thalamocortical neurons produce synchronized network oscillations of slow periodicity called spindle waves. The waves of electrical activity at 7–14 Hz wax and wane within a 1- to 3-s period and recur periodically once every 3–20 s (reviewed in refs. 2 and 5). Spindle waves are produced by the reciprocal interaction between inhibitory neurons of the thalamic reticular nucleus and excitatory thalamic relay neurons. The barrages of inhibitory postsynaptic potentials evoke Ca^{2+} rebounds by deinactivation of T type Ca^{2+} channels, which then, through the generation of trains of action potentials, reexcite the reticular cells. During the late stages of sleep, spindle waves are progressively replaced by oscillations with frequencies of 0.5–4 Hz. In contrast to origin of spindle oscillations in synaptic networks, the slow-frequency rhythm can be generated in single cells. HCN channels contribute to the different patterns of rhythmic activity of thalamocortical neurons in two ways. First, the interplay between low-threshold T type Ca^{2+} channels and HCN channels confers the autonomous 0.5- to 4-Hz rhythm onto thalamocortical relay cells (reviewed in refs. 2, 6, and 7). Activation of Ca^{2+} channels results in Ca^{2+} spikes and often in a high-frequency burst of Na^+/K^+ action potentials. Inactivation of Ca^{2+} channels terminates the Ca^{2+} spike, followed by hyperpolarization of the neuron and activation of hyperpolarization-activated channels that provide the depolarizing I_h current. Second, persistent activation of I_h during a spindle-wave epoch shifts the membrane potential by up to 5 mV to more positive values (5). This afterdepolarization stops oscillations, probably by inactivation of the T type Ca^{2+} channels (5). The duration of the refractory period in between spindle-wave epochs (3–20 s) is probably determined by the time course of I_h deactivation.

Recently, several members of the gene family of ion channels that carry I_h and I_f currents have been molecularly identified. In the following, we will adopt the nomenclature suggested by Clapham (*h*yperpolarization-activated and *c*yclic-*n*ucleotide-gated (HCN) channels; ref. 1): mHCN1 from mouse [mBCNG1 (8) and HAC2 (9)], mHCN2 [partial clone mBCNG2 (8) and HAC1 (9)], mHCN3 [partial clone mBCNG4 (8) and HAC3 (9)], and a putative fourth subtype mHCN4 [partial clone mBCNG3 (8)].

Two mouse clones, mHCN1 and mHCN2, have been functionally characterized by heterologous expression. Whereas HCN1 and HCN2 are both expressed in the thalamus, although not exclusively, their time course of activation (7, 8) is significantly faster than that of native HCN channels in thalamocortical neurons (9–12). Furthermore, at resting potentials of −60 mV to −68 mV (3), native HCN channels in thalamocortical neurons have a finite open probability (P_o) (2), whereas mHCN1 and mHCN2, owing to their negatively shifted midpoint potentials of activation ($V_{1/2} \leq -105$ mV), are practically closed at rest.

To molecularly identify the HCN channel subtype responsible for oscillatory activity in the thalamus, we screened a thalamus-specific cDNA library. Here we report the cloning and functional characterization of an HCN channel subtype from human (hHCN4). Significant expression of the hHCN4

The publication costs of this article were defrayed in part by page charge payment. This article must therefore be hereby marked "*advertisement*" in accordance with 18 U.S.C. §1734 solely to indicate this fact.

PNAS is available online at www.pnas.org.

Abbreviations: HCN channels, hyperpolarization-activated and cyclic-nucleotide-gated channels; $V_{1/2}$, potential of half-maximal activation; P_o, open probability; τ, time constant of activation.

Data deposition: The sequence reported in this paper has been deposited in the GenBank database (accession no. AJ238850).

†To whom reprint requests should be addressed. E-mail: r.seifert@fz-juelich.de.

message is observed in the heart, brain, and testis; within the brain, the thalamus is the predominant site of hHCN4 expression. Functional expression in a cell line produced channels with all of the hallmarks of HCN channels. However, hHCN4 differs from HCN1 and HCN2 by its unusually slow gating kinetics and voltage range of activation. The unique expression pattern and activation properties make hHCN4 a prime candidate for controlling the periodicity of oscillations in the thalamus and also for pacemaking in the heart.

MATERIALS AND METHODS

Cloning of Human hHCN4. A human thalamus cDNA library (CLONTECH, HL5009b) was screened with a DNA fragment that had been amplified by PCR from the library by using degenerate oligonucleotides corresponding to amino acid sequences EVFQPGD (residues 614–620) and DGSYFGE (residues 654–660). Several partial cDNA clones were isolated. Clone pB-HT60 [≈3.7 kilobase (kb)] contains the 5′-terminal region of hHCN4, including the 996-bp 5′ noncoding sequence. Seven stop codons were found in-frame upstream of the translation initiation site. A second overlapping clone pB-55HH4 (≈ 2.0 kb) contains sequences extending beyond the 3′ end of the coding region. The recombinant plasmid phHCN4 carrying the complete coding sequence for hHCN4 was constructed from these two overlapping clones by using standard procedures.

Northern Blotting. Northern blots of mRNA from various human tissues (CLONTECH) were hybridized with a ^{32}P-labelled PCR fragment (267 bp; corresponding to amino acids 728–816) at 68°C overnight in ExpressHyb hybridization solution (≈ 10^6 cpm/ml). Filters were washed with 2× SSC/0.05% SDS (4 × 10 min at room temperature) and with 0.1× SSC/0.1% SDS (2 × 20 min at 50°C). Autoradiography of labeled blots was performed for 2 weeks at −80°C.

Fluorescence *in Situ* Hybridization (FISH). For *in situ* hybridization, a 3,174-bp fragment of phHCN4 (corresponding to amino acids 195–1,203 and the 146-bp 3′ noncoding region) was biotin-labeled and used as a probe for chromosomal *in situ* suppression hybridization to human metaphase chromosomes as described (13). Labeled probe (80 ng) was combined with 3 μg of human Cot 1-DNA and 7 μg of salmon sperm DNA in a 10-μl hybridization cocktail. After hybridization to denatured human lymphocyte metaphase chromosomes overnight at 37°C and posthybridization washes, the biotinylated probes were detected via avidin-conjugated FITC. Chromosomes were counterstained with diamino-2-phenylindole (DAPI). Digitized images of DAPI staining and FITC were recorded separately by using a charge-coupled device camera (Photometrics), carefully aligned and electronically overlayed.

Functional Expression. Channel-specific cDNA was subcloned into the expression vector pcDNAIamp (Invitrogen) and expressed in HEK 293 cells as previously described (14). Currents were recorded with the patch-clamp technique in the whole-cell configuration. When necessary, leak currents were subtracted off-line by using steady-state currents between +10 and +50 mV. Experiments with caged cAMP were performed as described (15, 16). In the whole-cell configuration, the bath contained (in mM): 135 NaCl, 5 KCl, 1.8 $CaCl_2$, 2.8 $MgCl_2$ and 5 Hepes-NaOH at pH 7.4. The pipette solution contained (in mM): 126 KCl, 10 Hepes-KOH and 10 EGTA at pH 7.4. For experiments with cAMP, 50 μM NPE-caged cAMP was added to the pipette solution. cAMP was released from the caged form by illumination with light in the range of 320–400 nm. A UV light flash of similar intensity had no effect on currents in transfected and nontransfected HEK 293 cells in the absence of caged cAMP. All experiments were performed at room temperature (≈21°C).

RESULTS

Primary Structure of hHCN4. We isolated a clone phHCN4 from a human thalamus cDNA library (see *Materials and Methods*). The cDNA (4,751 bp) codes for a protein of 1,203 aa residues with a calculated molecular mass of 129.1 kDa. The deduced polypeptide sequence shows a high degree of similarity with previously cloned HCN channels: 63.6% identity with mouse HCN1; 69.4% identity with mouse HCN2; and 70.6% identity with mouse HCN3 (8–10). The sequence similarity is particularly pronounced in the transmembrane segments S1–S6, the pore region, and the cyclic nucleotide-binding domain. The N- and C-terminal domains of hHCN4 are significantly larger compared with mHCN1–mHCN3 (Fig. 1). Thus, hHCN4 represents a novel subtype of HCN channels. A partial clone of the mouse ortholog of hHCN4 has been previously reported by Santoro and coworkers (mBCNG3; ref. 8).

Tissue Distribution of hHCN4 mRNA Expression. Northern blot analysis showed strong expression of hHCN4 transcripts in heart (7.3 kb) and testis (7.3 kb and 4.5 kb) and a significantly weaker signal in total brain (7.3 kb; Fig. 2 *A* and *B*). However, analysis of the hHCN4 distribution within different regions of the human brain revealed a highly differential expression of the gene. Expression level of hHCN4 mRNA was highest in the thalamus, much lower in the substantia nigra, cerebellum, amygdala, and hippocampus, and not detectable in spinal cord, corpus callosum, or caudate nucleus (Fig. 2 *C* and *D*). The expression patterns of mouse and human HCN1 and human HCN2 are distinctively different from that of hHCN4 in that HCN2 mRNA is more uniformly expressed in all brain regions, and HCN1 mRNA is less abundant in the thalamus compared with other brain structures, e.g., hippocampus and amygdala (8, 10). Thus, hHCN4 may subserve a cellular function that is specific to thalamocortical neurons and of lesser importance for other brain regions (see *Discussion*).

The hHCN4 Gene Maps to Chromosome 15q24–q25. Hybridization of the human hHCN4 probe to metaphase chromosomes resulted in specific signals on human chromosome 15q24–q25 (Fig. 3). In 60% (18/30) of the evaluated metaphase cells, fluorescent signals were detected on both, and in 40% (12/30) on one, of the chromosome 15 homologs. No additional signals were found in other regions of the human genome in any of the experiments.

Functional Characterization. We studied the activity of hHCN4 channels in transfected HEK 293 cells with the patch-clamp technique in the whole-cell configuration. Hyperpolarizing steps in membrane potential, V_m, from a holding value of +10 mV to more negative test values (−50 to −150 mV) produced a small instantaneous current component followed by a slow time-dependent current that developed with a sigmoidal time course (Fig. 4*A*). Similar currents were not observed in nontransfected cells (data not shown).

The sigmoidal onset of currents indicates that the activation requires a series of conformational transitions involving both closed and open states (17). However, ignoring the sigmoidal onset of the current traces, the time course of activation was well described by a single exponential (as shown in Fig. 4*C*). The time constant of activation, τ, strongly depended on the test voltage (Fig. 4*B*, ●). Values for τ range from 265 ms (−150 mV) to 21.5 s (−70 mV). For comparison, the voltage dependence of the activation time constant τ measured at 36°C from thalamocortical neurons (taken from ref. 11) has been included (Fig. 4*B*, ▲). The difference in kinetics between native and hHCN4 channels is readily accounted for by the strong temperature dependence of the activation step: time constants at 36°C, calculated for the cloned channel from the data obtained at room temperature (assuming a Q_{10} of 6), perfectly coincide with the data for the native channel (Fig. 4*B*, ○).

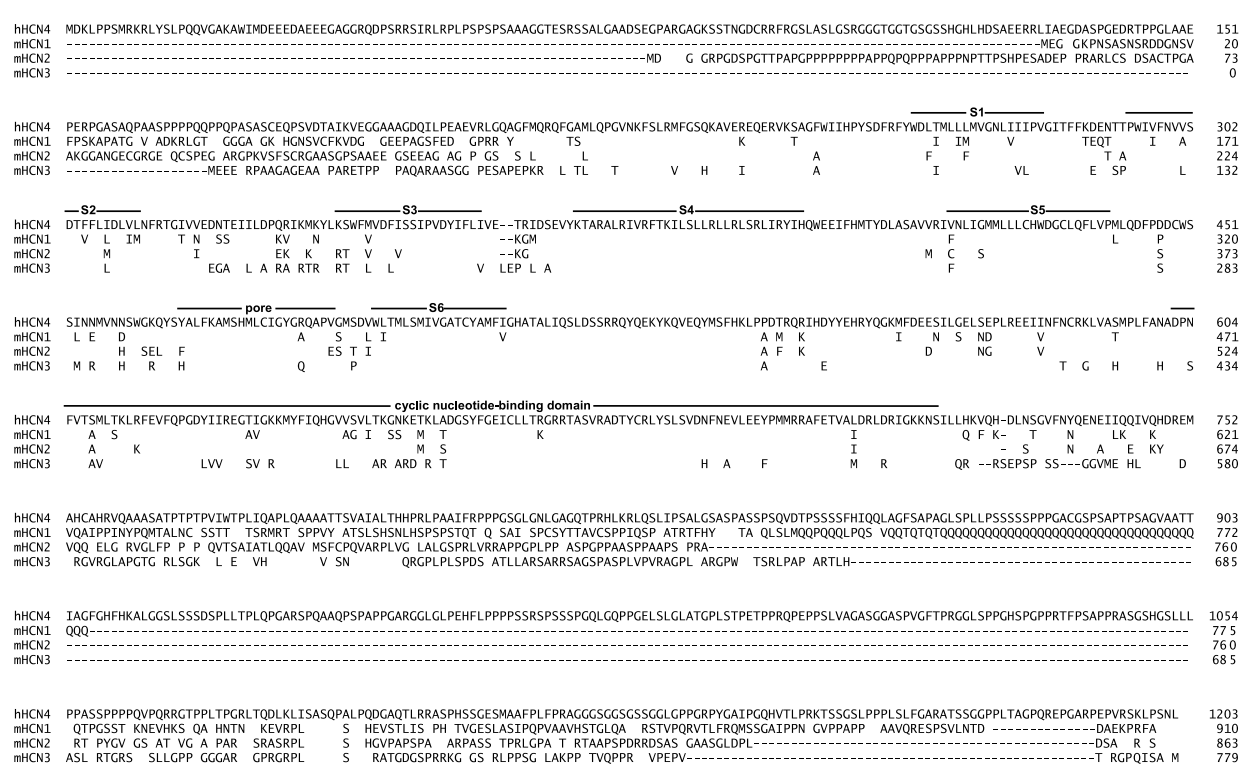

FIG. 1. Primary structure of the human HCN4 channel and sequence comparison with mouse subtypes mHCN1–mHCN3. Identical residues with respect to hHCN4 sequence are represented by empty spaces and gaps by dashes. The six predicted transmembrane segments (S1–S6), the pore region, and the cyclic nucleotide-binding domain are indicated by bars above the sequence. Sequences of mHCN1–mHCN3 are from ref. 9.

Because of the slow kinetics of the channel, P_o did not reach a steady state with the voltage protocols shown in Fig. 4 *A* and *C*. Nevertheless, the voltage dependence of the relative P_o taken from instantaneous tail currents was still satisfactorily described by Boltzmann functions (Fig. 4 *D* and *E*). However, the midpoint potential $V_{1/2}$ strongly depended on the duration of the hyperpolarizing voltage pulse and was shifted to the right for longer pulse durations (Fig. 4*E*). Fig. 4*F* summarizes these experiments. $V_{1/2}$ adopts very negative values for short pulses (i.e., 100 ms; $V_{1/2} = -182.1$ mV) and approaches a constant value of roughly -75 mV for very long pulses ($\geq$60 s).

The instantaneous current-voltage (I/V_m) relationship determined from tail currents was linear (Fig. 5 *A* and *B*). The mean reversal potential, V_{rev}, was -22.1 ± 3.4 mV (5 experiments) under nearly physiological gradients of monovalent ion concentrations.

To compare hHCN4-mediated currents in the presence and absence of cAMP in the same cell and to avoid slow effects such as cAMP-dependent phosphorylation, we used rapid photorelease of cAMP from caged derivatives (15, 18). Stepping V_m from 0 mV to -100 mV induced the characteristic rise in hHCN4 current (Fig. 6*A*). After the hyperpolarization-activated current reached a plateau, cAMP released by a short flash of UV light further increased the current amplitude. The time course of the cAMP-induced current increase was described by two exponentials of 182 ms (relative amplitude of 26%) and 1,633 ms (74%) (Fig. 6*A Inset*). Similar experiments with the cloned HCN channel from sea urchin sperm (16) and with a cyclic nucleotide-gated channel (15) yielded much faster rate constants. Thus, the hHCN4 channel displays inherently slow gating kinetics to changes in both membrane potential and cAMP concentration. We also compared the activation kinetics on steps to -120 mV before and after the photorelease of cAMP (Fig. 6*B*). The value for τ decreased almost 3-fold from 1,465 ms before the flash to 552 ms after the flash. Thus, for a given membrane potential, increasing the cAMP concentration produces a significant acceleration of the current activation.

The hydrolysis of photoreleased cAMP by endogenous phosphodiesterase activity was slow (see Fig. 6*E*) and enabled us to establish a complete P_o/V_m relationship with and without cAMP in one and the same cell. Mean values for $V_{1/2}$ were -85.2 ± 5.6 mV (13 cells) in the absence of cAMP and -74.1 ± 5.3 mV (10 cells) in the presence of cAMP for pulses of 7,500-ms duration (Fig. 6*C*). Thus, cAMP shifts the range of channel activation by 11 mV to more positive potentials.

Calculated values from the Boltzmann equation suggest that hHCN4 has a finite P_o at the resting potential of thalamocortical neurons. At -60 mV, relative P_o of hHCN4 adopts values from 5.7% to 31.6%, depending on the cAMP concentration of the cell. Moreover, at -40 mV, where HCN channels are believed to close, the relationship predicts a relative P_o of a few percent at saturating cAMP concentration. To verify this prediction, we used photorelease of cAMP from the caged derivative. The membrane potential of the cell was clamped to -40 mV. Because of the small P_o, in concert with an equally small driving force ($V_{rev} \approx -25$ mV) and the slow kinetics of the channel, we probed changes in P_o caused by liberation of cAMP by repetitively stepping the holding potential to $+50$ mV for 10 ms with an interpulse interval of 10 s. Because of its inherently slow gating kinetics, the hHCN4 channel does not deactivate during the short voltage pulse. The current amplitude at $+50$ mV was found to be stable for extended periods of time (Fig. 6*E*, see time interval 0–100 s). After the UV flash, the current amplitude increased, reflecting an increase in channel activity. Currents slowly returned to baseline levels that were not significantly different from levels before the flash. The slow decay of current amplitude reflects the clearance of cAMP from the cell by endogenous phosphodiesterase activity. This result demonstrates that hHCN4, even at significantly depolarized potentials, exhibits a measurable P_o. It has been proposed that the increase in $[Ca^{2+}]_i$ during spindle

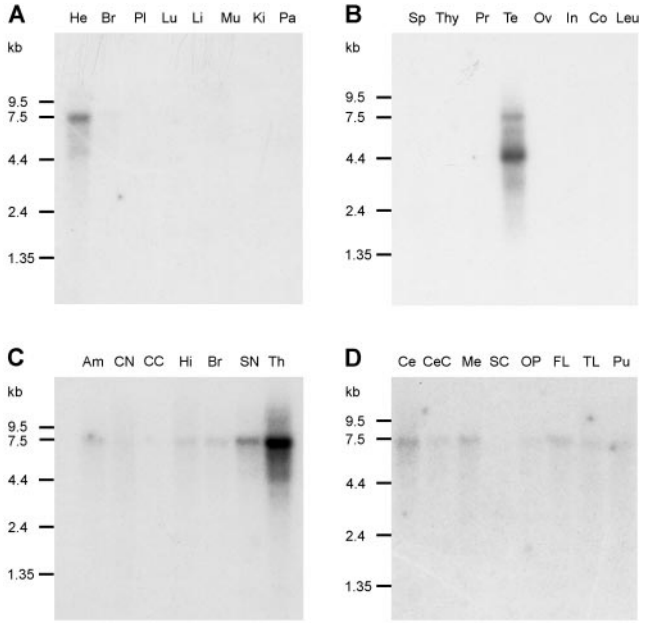

FIG. 2. Northern blot analysis of hHCN4 gene expression. Each lane contains 2 μg of poly(A)$^+$ RNA from each of the following human tissues: He, heart; Br, total brain; Pl, placenta; Lu, lung; Li, liver; Mu, skeletal muscle; Ki, kidney; Pa, pancreas (*A*); Sp, spleen; Thy, thymus; Pr, prostata; Te, testis; Ov, ovary; In, small intestine; Co, colon; Leu, peripheral blood leukocytes (*B*); Am, amygdala; CN, caudate nucleus; CC, corpus callosum; Hi, hippocampus; Br, total brain; SN, substantia nigra; Th, thalamus (*C*); and Ce, cerebellum; CeC, cerebral cortex; Me, medulla; SC, spinal cord; OP, occipital pole; FL, frontal lobe; TL, temporal lobe; Pu, putamen (*D*). Blots were hybridized with a ^{32}P-labeled 267-bp cDNA fragment.

episodes indirectly stimulates HCN channel activity by increasing cAMP concentration and thereby causes the afterdepolarization (5). Consequently, the time between episodes might be determined by the rate of cAMP hydrolysis by endogeneous phosphodiesterase activity. Fig. 6*E* shows that, in HEK cells, cAMP degradation slowly proceeds on a time scale that, given the lack of information on peak levels of cAMP and endogeneous phosphodiesterase activity in thalamocortical neurons, is not outrageously different from the rate at which the afterdepolarization decays.

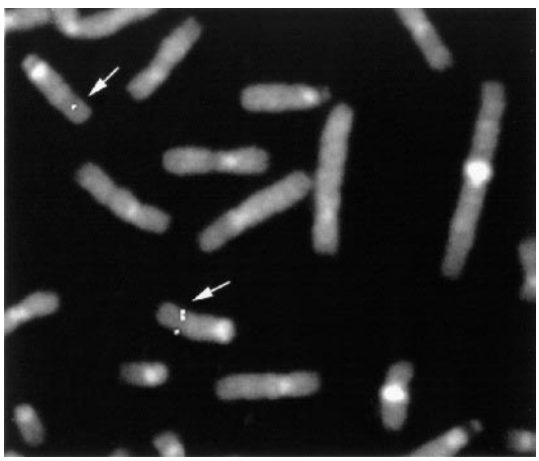

FIG. 3. Sections of human metaphase spreads after *in situ* hybridization with a biotinylated probe of hHCN4, detected with FITC conjugated to avidin. Arrows indicate the fluorescent signal on chromosome region 15q24–q25. Chromosomes were counterstained with DAPI.

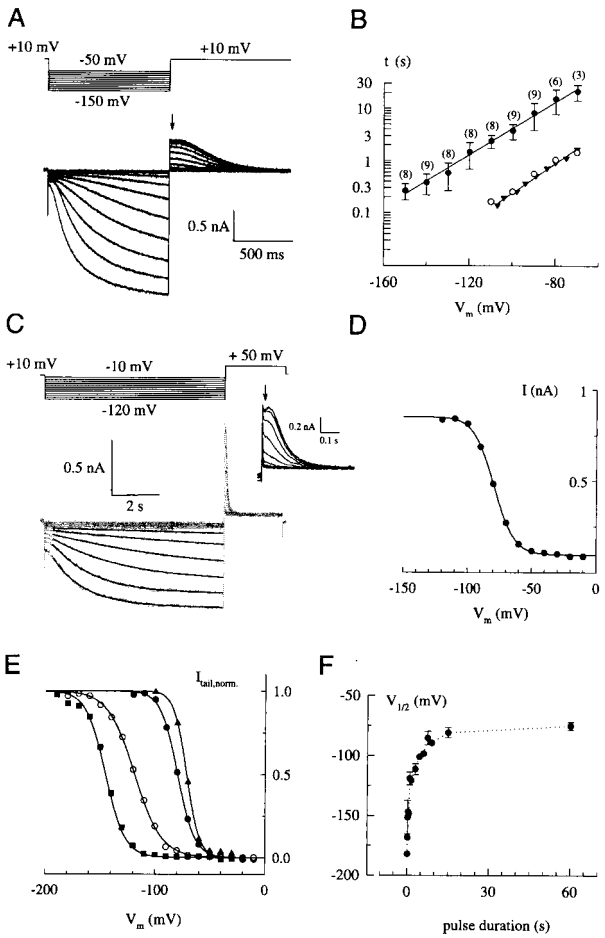

FIG. 4. Functional characterization of hHCN4. (*A*) Whole-cell current responses to hyperpolarizing voltage steps from a holding potential of +10 mV to test values between −50 and −150 mV in increments of 10 mV. Tail currents were recorded by stepping the voltage back to +10 mV. The arrow indicates the instantaneous tail current. (*B*) Voltage dependence of the activation rates. Time constants τ (±SD, ●) of current activation were determined by fitting single exponentials to the current traces of recordings as in *A* (−130 to −150 mV) and in *C* (all other voltages). The number of experiments is given in parentheses. Time constants of activation of native I_h currents (▲) recorded from thalamocortical neurons were taken from ref. 11; ○ represent time constants for hHCN4 at 36°C, calculated from the data at 21°C, assuming a $Q_{10} = 6$. (*C*) Whole-cell current responses to hyperpolarizing voltage steps (see protocol above the current traces) of 7,500 ms duration (gray traces) and superimposed fit with a single exponential function (solid lines). The *Inset* shows tail currents recorded at +50 mV on an expanded time scale. (*D*) Voltage dependence of instantaneous tail currents (●), taken from *C* (*Inset* , arrow), representing the relative P_o. Solid line is a fit of the Boltzmann function $(I - I_{min})/(I_{max} - I_{min}) = [1 - \exp([V - V_{1/2}]/s)]^{-1}$ with $V_{1/2} = -79.6$ mV and s = 7.9 to the data. (*E*) Normalized tail currents (symbols) and fits (solid lines) of experiments with varying duration t_p of the hyperpolarizing pulse: ■, t_p = 300 ms, $V_{1/2} = -151.4$ mV; ○, t_p = 1 s, $V_{1/2} = -119.0$ mV; ●, t_p = 7.5 s, $V_{1/2} = -85.2$ mV; ▲, t_p = 60 s, $V_{1/2} = -75.2$ mV. (*F*) Mean values ± SD for $V_{1/2}$ (determined as in *D* and *E*) plotted against duration of the hyperpolarizing pulse. $V_{1/2}$ saturates for long pulse durations (>60 s) at −75.2 (±3.4) mV.

DISCUSSION

In the human brain, hHCN4, unlike any other HCN channel subtype, is predominantly expressed in the thalamus. Moreover, hHCN4 and the native channel in thalamocortical neurons match in two functional features that set apart HCN channels from each other—midpoint potential $V_{1/2}$ and time constant τ of activation. First, the $V_{1/2}$ of activation of hHNC4 (−75.2 mV) is largely similar to that of I_h in thalamocortical

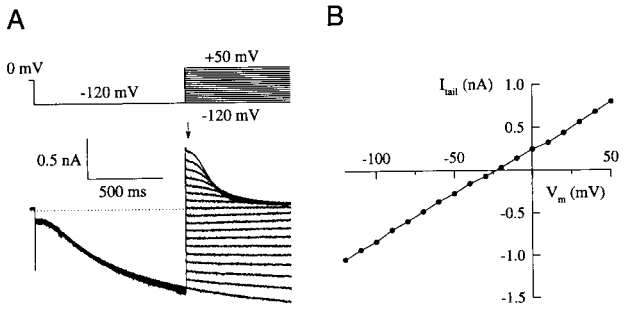

FIG. 5. (*A*) Current responses to hyperpolarizing voltage steps to −120 mV for 1 s and tail currents recorded by stepping the voltage to the indicated value (see voltage protocol above the current traces). The arrow indicates the instantaneous tail-current amplitudes used for the I/V_m relation shown in *B*. (*B*) Instantaneous I/V_m relation derived from tail currents in *A*. The reversal potential was −22 mV.

neurons (−74 to −85 mV; refs. 11, 12, and 19). A valid comparison of $V_{1/2}$ values is hampered by our observation that $V_{1/2}$ depends critically on the voltage protocol used. In particular, when working with a slowly gating HCN channel at room temperature, short voltage steps do not allow channel activation to come to completion and, therefore, the steady-state P_o derived from tail current amplitudes is seriously underestimated. As a consequence, the $V_{1/2}$ becomes shifted toward more negative values (see Fig. 4 *E* and *F*). For example, with 3-s pulses, the $V_{1/2}$ is shifted by 35 mV to more negative values compared with the $V_{1/2}$ at steady state. $V_{1/2}$ values reported in the literature for I_h and I_f currents are notoriously variable, and this variability has been attributed to different cAMP levels or to endogenous factor(s) that might be lost during recording in the whole-cell configuration or in exised patches (2, 4, 9, 16). We suggest that part of the large variability of $V_{1/2}$ values originates from using different pulse protocols. The resting potential of thalamocortical neurons (−60 to −68 mV; ref. 20) is distinctively more positive than the presumed K^+ equilibrium potential. Within this range of resting potentials, hHCN4 has a significant P_o and is expected to sustain a sizeable inward current that codetermines the resting potential. In fact, application of Cs^+, which blocks HCN channels, to thalamocortical neurons, causes hyperpolarization and an increase in apparent input resistance (11). In contrast to hHCN4, the $V_{1/2}$ of mHCN1 and mHCN2 have been reported to be distinctively more negative (−100 mV to −105 mV; refs. 8 and 9), and these channels would be practically closed in a neuron at rest.

Second, hHCN4 and native channels in thalamocortical neurons are rather similar in their relatively slow time course of activation, whereas mHCN1 and mHCN2 activate much faster. However, a meaningful comparison of kinetics must bear in mind the strong voltage and temperature dependence of activation. The time constant of activation of I_h in a neuron maintained at 36°C varies between ≈300 ms and ≈8.3 s, depending on V_m (11, 12), whereas mHCN1- and mHCN2-mediated currents at ambient room temperature activated with τ of ≈100–300 ms (8, 9). Taking into account the temperature dependence of the activation kinetics ($Q_{10} \approx 5$; ref. 21), at 36°C, activation rates of heterologously expressed mHCN1 und mHCN2 channels are expected to be even severalfold faster than at room temperature. In the same vein, the slower activation kinetics of cloned hHCN4 measured at room temperature compared with the native channel in thalamocortical neurons at 36°C (11) (see Fig. 4*B*) is fully accounted for by the difference in measuring temperature and a $Q_{10} \approx 6$. In conclusion, the unique expression pattern and activation properties suggest that hHNC4 encodes the pacemaker channel in thalamocortical neurons.

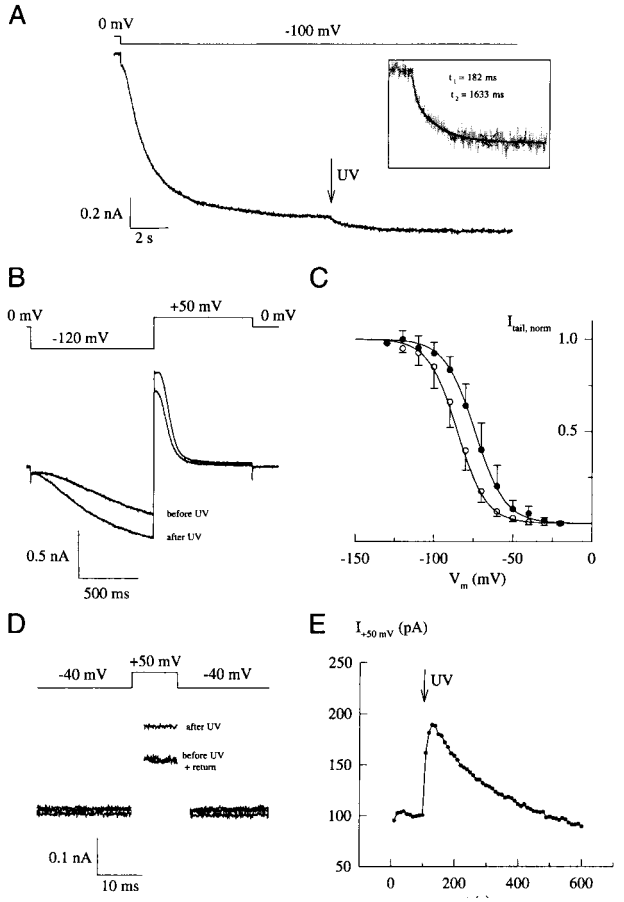

FIG. 6. Modulation of hHCN4-mediated currents by cAMP. (*A*) Incremental increase of steady-state current at −100 mV after photorelease of cAMP from caged cAMP. (*Inset*) Time course of flash-induced current increase displayed on a larger time scale. (*B*) Comparison of time courses of hHCN4 currents activated by steps to −120 mV before and after release of cAMP by the UV flash. (*C*) Voltage dependence of relative P_o derived from tail current analysis similar to that shown in Fig. 4 *C* and *D* in the absence (○) and presence (●) of cAMP. Midpoint potentials ($V_{1/2}$) and slope factors (*s*) were determined from a fit of the Boltzmann equation to the data. Mean $V_{1/2}$ (control) = −85.2 ± 5.6 mV; s = 9.2 ± 1.9 mV (13 experiments); mean $V_{1/2}$ (cAMP) = −74.1 ± 5.3 mV; s = 9.7 ± 2.1 mV (10 experiments). (*D*) Demonstration of open hHCN4 channels at a depolarized potential (−40 mV). From a holding voltage of −40 mV, short voltage pulses of 10-ms duration to +50 mV were repetetively applied every 10 s. After 100 s, a flash of UV light (500 ms) was applied, releasing cAMP from the caged compound. Three example traces are shown at t = 100 s, t = 140 s, and t = 550 s. Capacitive current transients have been removed for clarity. (*E*) Rise and decay of flash-induced changes in current amplitude measured at +50 mV in *D*.

At least two HCN channel subtypes (HCN2 and HCN4) are expressed in the thalamus in appreciable amounts. We envisage three different scenarios. First, HCN2 and HCN4 altogether may reside in different cell populations of the thalamus. Second, the native channel may comprise two distinct subunits, and the HCN4 subunit may determine the activation kinetics of the heterooligomeric complex. Finally, thalamocortical neurons may be furnished with two different HCN channel populations that operate within distinct regimes of membrane potential. In thalamocortical neurons, the time course of I_h has been described by a single (11, 12) or two (22) kinetic components. Moreover, investigations of I_h in cortical neurons have indicated that the time course of I_h may be best approximated by the sum of two kinetic components (23, 24). It remains to be established whether multiphasic time courses originate from distinct channel populations or reflect multiple

gating processes within the same channel population. It will be important for future work to study the molecular composition and cellular distribution of HCN channel subtypes in thalamic areas of the brain. Aside from the thalamus, the substantia nigra represents the brain structure with the highest expression level of hHCN4. Neurons within this area are also characterized by rhythmic activity that involves relatively slowly activating I_h currents (25–27).

The high expression level in heart tissue suggests that hHCN4 may also encode the principal pacemaker channel in the human heart. The intriguingly similar activation kinetics of I_f in myocytes of the sinoatrial node and cardiac Purkinje fibers (28–30) and of hHCN4 certainly support this conclusion. However, the activation threshold of I_f in cardiac Purkinje fiber is distinctively more negative than in the sinoatrial node (29, 31).

The strong hybridization signal with testis mRNA suggests that hHCN4 is also expressed in mature spermatozoa or their precursor cells. In this respect, hHCN4 may represent the mammalian equivalent to the HCN channel in the flagellum of sea urchin spermatozoa (16). Although the functional significance of pacemaker channels in spermatozoa is not known, both the sea urchin channel and hHCN4 may be involved in the generation of rhythmic activity that controls the waveform of flagellar beating. In fact, spermatogenic cells comprise an assortment of channels that is astoundingly similar to that of bursting neurons. A low-threshold T type Ca^{2+} channel and a pH-sensitive K^+ channel, which belongs to the family of Ca^{2+}-dependent K^+ channels, have been described in mammalian spermatogenic cells (32–34). In hyperactive hamster spermatozoa, oscillations of intracellular Ca^{2+} have been reported (35), demonstrating that spermatozoa are capable to sustain rhythmic patterns of activity. The motility of spermatozoa is also controlled by intracellular pH_i (for review, see ref. 36). In this respect, it is of particular physiological significance that intracellular alkalization shifts the $V_{1/2}$ of the thalamocortical HCN channel by 4–5 mV to more positive values (37). Therefore, in mammalian spermatozoa, both pH-dependent K^+ channels and HCN4 channels may mediate the physiological responses triggered by a change in pH_i. In conclusion, similar molecular components may underlie rhythmic activity of cells as diverse as bursting neurons and swimming spermatozoa.

The hHCN4 gene was mapped to 15q24–q25. Several diseases have been mapped to this chromosomal locus. A syndrome of severe mental retardation, spasticity, and tapetoretinal degeneration is linked to chromosomal locus 15q24 (38). A second disorder, which is also linked to chromosome 15q24, is an autosomal-dominant nocturnal frontal-lobe epilepsy (ADNFLE) (39). Future work is required to show whether mutations in the hHCN4 gene cause these diseases. Note. After submission of this manuscript, two papers appeared on the cloning of HCN4 from rabbit (40) and human heart (41). The rabbit cDNA probably represents a partial clone that is lacking part of the N-terminal region.

We thank Prof. H. zur Hausen for support. This work was supported by the Deutsche Forschungsgemeinschaft (U.B.K).

1. Clapham, D. E. (1998) *Neuron* **21,** 5–7.
2. Pape, H.-C. (1996) *Annu. Rev. Physiol.* **58,** 299–327.
3. Lüthi, A. & McCormick, D. A. (1998) *Neuron* **21,** 9–12.
4. DiFrancesco, D. (1993) *Annu. Rev. Physiol.* **55,** 455–472.
5. Bal, T. & McCormick, D. A. (1996) *Neuron* **17,** 297–308.
6. Steriade, M., McCormick, D. A. & Sejnowski, T. J. (1993) *Science* **262,** 679–685.
7. Lüthi, A. & McCormick, D. A. (1998) *Neuron* **20,** 553–563.
8. Santoro, B., Liu, D. T., Yao, H., Bartsch, D., Kandel, E. R., Siegelbaum, S. A. & Tibbs, G. R. (1998) *Cell* **93,** 717–729.
9. Ludwig, A., Zong, X., Jeglitsch, M., Hofmann, F. & Biel, M. (1998) *Nature (London)* **393,** 587–591.
10. Santoro, B., Grant, S. G. N., Bartsch, D. & Kandel, E. R. (1997) *Proc. Natl. Acad. Sci.USA* **94,** 14815–14820.
11. McCormick, D. A. & Pape, H.-C. (1990) *J. Physiol. (London)* **431,** 291–318.
12. Soltesz, I., Lightowler, S., Leresche, N., Jassik-Gerschenfeld, D., Pollard, C. E. & Crunelli, V. (1991) *J. Physiol. (London)* **441,** 175–197.
13. Lichter, P., Tang, C. C., Call, K., Hermanson, G., Evans, G. A., Housman, D. & Ward, C. D. (1990) *Science* **247,** 64–69.
14. Baumann, A., Frings, S., Godde, M., Seifert, R. & Kaupp, U. B. (1994) *EMBO J.* **13,** 5040–5050.
15. Hagen, V., Dzeja, C., Frings, S., Bendig, J., Krause, E. & Kaupp, U. B. (1996) *Biochemistry* **35,** 7762–7771.
16. Gauss, R., Seifert, R. & Kaupp, U. B. (1998) *Nature (London)* **393,** 583–587.
17. DiFrancesco, D. (1999) *J. Physiol. (London)* **515,** 367–376.
18. Kaupp, U. B., Dzeja, C., Frings, S., Bendig, J. & Hagen, V. (1998) *Methods Enzymol.* **291,** 415–430.
19. Budde, T., Biella, G., Munsch, T. & Pape, H.-C. (1997) *J. Physiol. (London)* **503,** 79–85.
20. Pape, H.-C. & McCormick, D. A. (1989) *Nature (London)* **340,** 715–718.
21. Halliwell, J. V. & Adams, P. R. (1982) *Brain Res.* **250,** 71–92.
22. Williams, S. R., Turner, J. P., Hughes, S. W. & Crunelli, V. (1997) *J. Physiol. (London)* **505,** 727–747.
23. Solomon, J. S., Doyle, J. F., Burkhalter, A. & Nerbonne, J. M. (1993) *J. Neurosci.* **13,** 5082–5091.
24. Solomon, J. S. & Nerbonne, J. M. (1993) *J. Physiol. (London)* **469,** 291–313.
25. Kang, Y. & Kitai, S. (1993) *Neurosci. Res.* **18,** 209–221.
26. Cathala, L. & Paupardin-Tritsch, D. (1999) *Eur. J. Neurosci.* **11,** 398–406.
27. Cathala, L. & Paupardin-Tritsch, D. (1997) *J. Physiol. (London)* **503,** 87–97.
28. DiFrancesco, D. & Tortora, P. (1991) *Nature (London)* **351,** 145–147.
29. DiFrancesco, D. (1984) *J. Physiol. (London)* **348,** 341–367.
30. Maruoka, M., Nakashima, Y., Takano, M., Ono, K. & Noma, A. (1994) *J. Physiol. (London)* **427,** 437–443.
31. Callewaert, G., Carmeliet, E. & Vereeke, J. (1984) *J. Physiol. (London)* **349,** 643–661.
32. Arnoult, C., Zeng, Y. & Florman, H. M. (1996) *J. Cell Biol.* **134,** 637–645.
33. Liévano, A., Santi, C. M., Serrano, C. J., Treviño, C. L., Bellvé, A. R., Hernández-Cruz, A. & Darszon, A. (1996) *FEBS Lett.* **388,** 150–154.
34. Schreiber, M., Wei, A., Yuan, A., Gaut, J., Saito, M. & Salkoff, L. (1998) *J. Biol. Chem.* **273,** 3509–3516.
35. Suarez, S. S., Varosi, S. M. & Dai, X. (1993) *Proc. Natl. Acad. Sci. USA* **90,** 4660–4664.
36. Ward, C. R. & Kopf, G. S. (1993) *Dev. Biol.* **158,** 9–34.
37. Munsch, T. & Pape, H. C. (1999) *J. Physiol. (London)*, in press.
38. Mitchell, S. J., McHale, D. P., Campbell, D. A., Lench, N. J., Mueller, R. F., Bundey, S. E. & Markham, A. F. (1998) *Am. J. Hum. Genet.* **62,** 1070–1076.
39. Phillips, H. A., Scheffer, I. E., Crossland, K. M., Bhatia, K. P., Fish, D. R., Marsden, C. D., Howell, S. J. L., Stephenson, J. B. P., Tolmie, J., Plazzi, G., *et al.* (1998) *Am. J. Hum. Genet.* **63,** 1108–1116.
40. Ishii, T. M., Takano, M., Xie, L. H., Noma, A. & Ohmosi, H. (1999) *J. Biol. Chem.* **274**, 12835–12839.
41. Ludwig, A., Zong, X., Stiebes, J., Hullin, R., Hofmann, F. & Biel, M. (1999) *EMBO J.* **18**, 2323–2329.